Sediment Transport and Deposition from a Two-Layer Fluid Model of Gravity Currents on Sloping Bottoms

By T. B. Moodie, J. P. Pascal, and G. E. Swaters

This article reports on a theoretical and numerical study of noneroding turbulent gravity currents moving down mildly inclined surfaces while depositing sediment. These flows are modeled by means of two-layer fluid systems appropriately modified to account for the presence of a sloping bottom and suspended sediment in the lower layer. A detailed scaling argument shows that when the density of the interstitial fluid is slightly greater than that of the ambient and the suspension is such that its volume fraction is of the order of the aspect ratio squared, for low aspect ratio flows a two-layer shallow-water theory is applicable. In this theory there is a decoupling of particle and flow dynamics. In contrast, however, when the densities of interstitial and ambient fluids are equal, so that it is the presence of the particles alone that drives the flow, we find that a consistent shallow-water theory is impossible no matter how small the aspect ratio or the initial volume fraction occupied by the particles. Our two-layer shallow-water formulation is employed to investigate the downstream evolution of flow and depositional characteristics for sloping bottoms. This investigation uncovers a new phenomenon in the formation of a rear compressive zone giving rise to shock formation in the post-end-wall-separation phase of the particle-bearing gravity flow. This separation of flow from the end wall in these fixed volume releases differs from what has been observed on horizontal surfaces where the flow always remains in contact with the end wall.

Address for correspondence: Professor T. B. Moodie, Applied Mathematics Institute, Department of Mathematical Sciences, University of Alberta, Edmonton, Alberta T6G 2G1, Canada.

STUDIES IN APPLIED MATHEMATICS 100:215–244

Published by Blackwell Publishers, 350 Main Street, Malden, MA 02148, USA, and 108 Cowley Road, Oxford, OX4 1JF, UK.

1. Introduction

A gravity current consists of the flow of one fluid within another when this flow takes place because of relatively small differences in density between the fluids [1]. Such gravity flows constitute a class of very complex flows, more complex, for example, than open-channel flows such as rivers.

Gravity currents are primarily horizontal, occurring as either top or bottom boundary currents or as intrusions at some intermediate level. Turbidity currents are gravity currents in which the excess density or unit weight providing the driving buoyancy force is due to the presence of sediment being held in suspension by fluid turbulence. Thus whether or not a sediment-bearing gravity current is a turbidity current will depend to a great extent upon the ordering that exists between the density of the interstitial (suspending) fluid and that of the ambient fluid. For example, in the case of a bottom particle-bearing gravity current whose interstitial fluid has a density that is equal to or less than that of the ambient, the driving buoyancy forces are due solely to the presence of suspended particles and we have a turbidity current. In this case it is possible that particle settling may lead to a reduction in bulk density of the bottom flow thereby transforming the bottom current into an intrusive turbidity current at some neutrally buoyant intermediate depth [2]. Further particle settling can subsequently lead to complete buoyancy reversal, the initiation of a buoyant plume, and the creation of a surface gravity current [3] in which the remaining particles play no role in the dynamics. On the other hand, should the density of the interstitial fluid in the bottom current be greater than that of the ambient, then the turbidity and/or particle-bearing gravity current will remain buoyantly stable throughout the particle-settling phase. If this suspension is either initially or becomes sufficiently dilute through the settling of particles, then there will be a stage when these particles will play little or no role in the dynamics of the flow. The flow dynamics will be governed by the density difference that exists between interstitial and ambient fluids and we have a particle-bearing gravity current.

These turbidity and/or particle-bearing gravity currents with their potentially extremely complex dynamics occur in a vast array of natural and human-made settings. A relatively complete catalogue of events in which they play a role is to be found in [4]. They are of particular interest to oceanographers and geologists in that the abyssal plains of many oceans consist of sand and silt layers that appear to have come from the continental shelf, transported in the form of turbidity currents. Many sandstones previously believed to have been deposited in shallow water over long time periods were in fact deposited rather precipitously by turbidity currents in water thousands of meters deep [1]. These turbidity currents may be initiated when an unstable submarine shelf near a coastline collapses, resulting

in a submarine landslide. This landslide entrains fluid as it moves downslope and this fluid suspends sediment and, when it reaches the basal plain, spreads as a gravity current depositing its sediment. These gravity currents have been observed, in their self-stoking phase, to travel at speeds in excess of 20 m s^{-1} over distances of hundreds of kilometers [4, 5]. However, since direct observations of high-velocity gravity flows in nature are extremely rare, it is by employing models that we can hope to attain some understanding of the mechanisms that govern this important class of phenomena.

It is in this spirit that we present our model for the downslope deposition of particles from monodisperse particle-bearing gravity currents. This classification that sees a difference between what we call particle-bearing gravity currents and particle-driven turbidity currents is somewhat arbitrary as there will be a spectrum of behaviors for nonhomogeneous gravity currents. That is, even for dilute suspensions the particles may exert some minor influence on the dynamics of the flow. However, turbidity currents, as opposed to particle-bearing gravity currents, are not possible without the dynamical influence of the suspended particles on the flow. Whether this influence is dominant or not must be decided on a case-by-case basis and is a subtle issue that has implications for the use of shallow-water theory. One of the principal conclusions of this article and one that may have major repercussions in the current turbidity literature is that turbidity currents cannot be described in terms of shallow-water theory. In transparent language this finding says that if particles and their settling process drive the flow then vertical structure in the horizontal velocity field is unavoidable.

The majority of the theoretical work on gravity currents from the early calculation by von Kármán [6] up to that by Benjamin [7] and right on through into the mid 1980s treated the gravity current as steady, existing in either an inertia-buoyancy or, at later stages in the flow, in a viscous-buoyancy balance and finally, in the very late stages of the flow, in a viscous-surface-tension balance [8]. Notable exceptions were the works of Hoult [9] and Fannelop and Waldman [10], in which governing equations were established and subsequently solved rather than seeking time-independent force balances. Hoult's formulation for bottom flows has the advantage over Huppert's [11] because it includes the effects of motion of the lighter upper fluid: a requirement when the depth of the bottom current is comparable to the depth of the overlying fluid [12, 13]. Hoult's [9] solution (and Huppert's [11]) was obtained in terms of a similarity variable and so the derived relationships are valid only after sufficient time has elapsed, since release of the fixed volume of fluid, for the initial geometry of that volume to be irrelevant. With our focus being on the early post-release period and attendant transient nonlinear evolution of the well-mixed fixed volume suspension and its associated depositional patterns, these "far-field" methods are not employed here.

Further in the realm of time-dependent homogeneous gravity flow studies is the work of Rottman and Simpson [14] on instantaneous releases of bottom gravity flows. In a series of detailed experiments they studied instantaneous releases for $0 < h_0/H \leq 1$, where h_0 is the initial depth of the released heavy fluid and H the total depth of the fluid in the channel. In their work they concentrated on the important issue of the flow's transition to the self-similar phase. The key feature of their observations was that for h_0/H equal to or slightly less than unity, the disturbance generated at the end wall has the appearance of an internal hydraulic drop whereas for smaller values of h_0/H ($\lesssim 0.7$) it is a long wave of depression. These experiments served to emphasize the importance of including the effect of the ambient fluid on the gravity current when that current is a sensible fraction of the total depth. As a possible framework for discussing these experiments they solved an initial value problem for the two-layer, shallow-water equations using the method of characteristics. Their interpretation of the experimental results in terms of the numerical simulations gives, at best, a qualitative understanding for $0 < h_0/H < \frac{1}{2}$. However, for $h_0/H > \frac{1}{2}$ there is little resemblance between their numerical simulations and the experimentally observed transition of the flow to the self-similar phase. D'Alessio et al. [13] employed a two-layer shallow-water model to study sudden releases for fixed volumes entering a lighter ambient fluid as a bottom gravity flow. Using MacCormack's method [15] to integrate numerically the hyperbolic system they were able to achieve very good agreement with the experimental results of Rottman and Simpson [14] for transition to self-similarity. Also, employing multiple scales arguments they were able to show analytically the dependence of internal bore formation on initial fraction depth of the release volume. The experimentally observed slowing down of the front as the internal bore overtakes it is captured by their model. Grundy and Rottman [16], in their study of the approach to self-similarity for solutions to the shallow-water equations for sudden releases of fixed volumes, employed a set of model equations that ignored inertial effects due to the presence of the lighter ambient fluid. Their subsequent numerical studies for plane flow show little resemblance to the observed flows of Rottman and Simpson [14]. Bonnecaze et al. [12] employing a two-step Lax–Wendroff scheme to solve the problem of sudden release of a fixed volume of homogeneous heavy fluid on a horizontal bottom achieved very good qualitative agreement with the experiments of Rottman and Simpson [14] when they took into account the inertial effects of the ambient fluid.

In stark contrast to the large body of both theoretical and experimental literature on homogeneous gravity currents, the amount of published work on sediment-bearing flows is relatively meager. If we further refine our search to look for models having the capacity to predict the downstream

evolutionary characteristics of deposits, then the literature is indeed sparse. The reason for this may be that to predict this downstream evolution requires consideration of the behavior of an entire surge rather than merely the behavior at a point in an otherwise horizontally infinite flow [5]. If we refine our search still further to look for the natural inclusion of a variable slope bottom then we will find that only the most primitive models have been developed.

Attempts at theoretical studies of the overall time-dependent interaction between flow and sedimentation for gravity currents are very recent. These commenced with the works of Sparks et al. [17], Bonnecaze et al. [12, 18], and Dade et al. [5, 19]. In these articles are presented both theory and experiment for bottom turbidity currents on horizontal and uniformly sloping bottoms in the depositional regime. For horizontal bottoms the models are based upon a form of shallow-water theory in the Boussinesq limit modified for the presence of dilute vertically homogeneous particle suspensions in the absence of viscosity. While for sloping bottoms the sustained propagation of a sediment-laden cloud that maintains a constant shape is considered to result from the drive of the downslope component of buoyancy and not from self-weight collapse. These articles treat sudden fixed volume releases with reversing buoyancy leading to buoyant plume formation [17], fixed volume releases with neutral buoyancy as the long-time particle-free state [12], fixed volume releases, and the constant flux of a suspension for axisymmetric flows [18], gravity surges, and deposition on uniform slopes with entrainment of ambient seawater and the effect of seafloor friction included [5] and nonentraining suspension-bearing gravity surges on horizontal surfaces [19].

In this article we present a complete and rigorous development of model equations for studying the downslope depositional patterns from dilute, monodisperse particle-suspension gravity currents produced by sudden fixed volume releases of well-mixed suspensions. In all cases the lighter ambient fluid is taken to have finite depth with its upper surface free.

The model to be developed here starts from two-layer fluid theory modified to take into account a variably sloping bottom and suspended particles in the lower layer. We assume, as in [12, 18], that the flow is two-dimensional, that the particles are vertically well mixed by turbulence, and that particles are not entrained into the lower layer but settle out with equal settling velocities that are much less than the flow speed. Also, since a stable density gradient strongly inhibits turbulent mixing [20], we ignore entrainment of the ambient homogeneous fluid into the bottom gravity current. Our focus is on the situation in which the interstitial fluid has a density that is slightly greater than that of the ambient fluid. This model therefore has relevance either to saline currents carrying particles into fresh water or to the study of lakes and reservoirs where, because of the low

sediment concentration, temperature may be as important in forming gravity flows as suspended sediment.

We commence our theoretical work by developing the complete coupled two-layer fluid equations for a bottom suspension-bearing gravity current on a sloping bottom underlying a homogeneous fluid. We then carry out a systematic scaling of these equations in order to ascertain in what circumstances shallow-water theory may be employed. From previous analyses of homogeneous fluids [21] it is known that shallow-water theory depends upon the smallness of the aspect ratio $\delta \equiv H/L$, where L is a horizontal scale of the motion and H the depth that is assumed to characterize the vertical scale of the motion. The smallness of the aspect ratio for homogeneous fluids is *sufficient* to guarantee that the horizontal velocity field is independent of the vertical coordinate. To achieve this absence of vertical structure in the horizontal velocity field for a heterogeneous fluid of the type being analyzed here we find that it is *sufficient* that δ as well as a parameter characterizing the volume fraction occupied by suspended particles both be small. Our results appear to be in conflict with those of Bonnecaze et al. [12, 18] and also Sparks et al. [17] since to achieve shallow-water theory by means of consistent scaling arguments we find that the particle concentration cannot influence flow dynamics. That is, the fluid momentum equations and the equation for particle conservation are, to leading order, decoupled. This result was anticipated by Dade and Huppert [19]. The details of this model development are presented in Section 2, together with some further discussion concerning other models and their applicability. Section 3 is devoted to a numerical study of fixed volume releases wherein we explore the influence of bottom slope and initial fractional depth on the flow and depositional patterns. Our numerical results are achieved using a relaxation scheme for conservation laws developed recently by Jin and Xin [22]. Our final section contains a discussion of results and some further comments on shallow-water theory.

2. Model development

Consider a gravity current produced by the release of a well-mixed suspension of bulk density ρ into an ambient fluid of lesser density ρ_1 overlying a sloping bottom. The physical configuration is depicted in Figure 1, where $\eta(x,t)$ represents the displacement of the free surface from its undisturbed configuration, ρ_2 is the density of the interstitial fluid supporting the particles of density ρ_3. $\mathbf{u} = (u,w)$ is the fluid velocity in Cartesian coordinates with position vector $\mathbf{x} = (x,z)$, H is a vertical-length scale, $h(x,t)$ is the thickness of the bottom gravity current, and the variable bottom is located at $z = -sf(x)$, where s $(0 < s \ll 1)$ is a nondimensional parameter.

The flow is driven by the buoyancy forces arising because of the difference between the bulk density ρ of the suspension and the density of the ambient fluid, ρ_1. The density of the suspension, which may vary along its length, is the local volume average of the particle density ρ_3 and the density ρ_2 of the interstitial fluid and is given by

$$\rho(\varphi) = \rho_3\varphi + (1-\varphi)\rho_2, \tag{2.1}$$

where $\varphi = \varphi(x,t)$ is the volume fraction occupied by the particles ($0 < \varphi \ll 1$). With dilute suspensions terms $\boldsymbol{O}(\varphi)$ can be neglected in the continuity equation for the particle-bearing gravity current to give for mass conservation in the upper (homogeneous) and lower layers

$$\frac{\partial u_1}{\partial x} + \frac{\partial w_1}{\partial z} = 0, \tag{2.2}$$

$$\frac{\partial u_2}{\partial x} + \frac{\partial w_2}{\partial z} = 0, \tag{2.3}$$

respectively. In all that follows we further assume that the Reynolds number of the flow is sufficiently large ($\sim 10^3$) that viscous forces are negligible and that the flow dynamics are dominated by a balance between buoyancy and inertial forces. The equation of momentum balance in each layer then takes the form

$$\rho\frac{D}{Dt}\mathbf{u} = -\nabla p + \rho\mathbf{g}, \tag{2.4}$$

wherein p is the total fluid pressure and $\mathbf{g}$ the gravitational acceleration with ρ for the lower layer taking the variable value $\rho(\varphi)$ specified by (2.1). We now adapt Equations (2.2)–(2.4) to study low-aspect ratio flows involving two coupled layers consisting of a homogeneous fluid surrounding a dilute

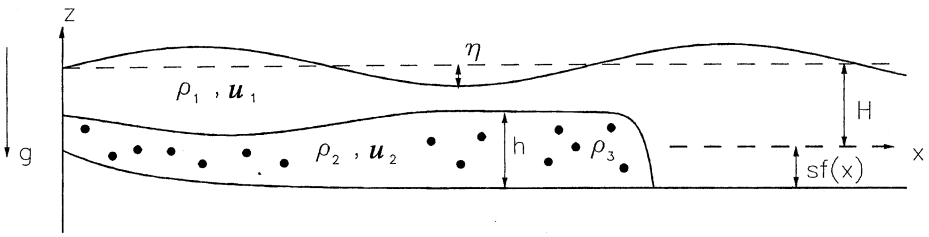

Figure 1. Geometry of the two-layer model used in this article.

suspension overlying a sloping bottom. Throughout our development we keep the upper surface free.

The momentum equations for the upper (homogeneous) layer may be written as

$$\frac{\partial u_1}{\partial t} + u_1 \frac{\partial u_1}{\partial x} + w_1 \frac{\partial u_1}{\partial z} = -\frac{1}{\rho_1} \frac{\partial p_1^*}{\partial x}, \tag{2.5}$$

$$\frac{\partial w_1}{\partial t} + u_1 \frac{\partial w_1}{\partial x} + w_1 \frac{\partial w_1}{\partial z} = -\frac{1}{\rho_1} \frac{\partial p_1^*}{\partial z}, \tag{2.6}$$

where the total pressure in the upper layer has been expressed as

$$p_1 = -\rho_1 g z + p_1^*(x, z, t) \tag{2.7}$$

with p_1^* representing the dynamic pressure field in the upper layer. This decomposition allows us to eliminate the constant gravitational force per unit mass from the vertical momentum equation (2.6).

The momentum equations for the lower (inhomogeneous) layer are

$$\rho(\varphi)\left(\frac{\partial u_2}{\partial t} + u_2 \frac{\partial u_2}{\partial x} + w_2 \frac{\partial u_2}{\partial z} \right) = -\frac{\partial p_2}{\partial x}, \tag{2.8}$$

$$\rho(\varphi)\left(\frac{\partial w_2}{\partial t} + u_2 \frac{\partial w_2}{\partial x} + w_2 \frac{\partial w_2}{\partial z} \right) = -\frac{\partial p_2}{\partial z} - \rho(\varphi) g. \tag{2.9}$$

Writing the bulk density ρ in the form

$$\rho(\varphi) = \rho_2 + \varphi(x,t)(\rho_3 - \rho_2) \tag{2.10}$$

and the total pressure field as

$$p_2(x, z, t) = \rho_1 g H - \rho_2 g z + p_2^*(x, z, t) \tag{2.11}$$

transforms the momentum equations into

$$\frac{\partial u_2}{\partial t} + u_2 \frac{\partial u_2}{\partial x} + w_2 \frac{\partial u_2}{\partial z} = -\frac{1}{\rho_2} \frac{\partial p_2^*}{\partial x}, \tag{2.12}$$

$$\frac{\partial w_2}{\partial t} + u_2 \frac{\partial w_2}{\partial x} + w_2 \frac{\partial w_2}{\partial z} = -\frac{1}{\rho_2} \frac{\partial p_2^*}{\partial z} - \varphi \frac{(\rho_3 - \rho_2)}{\rho_2} g. \tag{2.13}$$

The decomposition in (2.11) enables us to eliminate the constant part of the gravitational force per unit mass from the vertical momentum equation but

not the variable part that depends upon the volume fraction $\varphi(x,t)$. We have also employed a Boussinesq approximation in eliminating terms $O(\varphi)$ except where they are multiplied by g.

We require an additional equation describing the conservation of particles in the lower layer. In deriving this equation we assume that the particles are vertically well mixed by the turbulence in the current, dilute, noncohesive, that they are advected by the mean flow, and that they settle out through the viscous sublayer at the bottom of the current with equal settling velocities. Applying conservation principles to an arbitrary segment of the flow regime $x_2 < x < x_1$ leads directly to

$$\frac{\partial}{\partial t}(h\rho_3\varphi) + \frac{\partial}{\partial x}\left(\int_{-sf(x)}^{h(x,t)-sf(x)} \rho_3\varphi u_2\, dz\right) + \rho_3\varphi x_s = 0, \qquad (2.14)$$

where v_s denotes the Stokes settling velocity of an isolated particle [12].

We now focus on Equations (2.5), (2.6), (2.12), (2.13), and (2.14) with the goal of developing a set of equations describing low-aspect ratio flows in each layer with the lower layer comprising a dilute suspension. Although it is obviously the case that the initial flow following release of a gravity current of finite volume is a complex three-dimensional unsteady flow, soon after release the current will have spread sufficiently that its length is very much greater than its height. The height will at this stage be *slowly varying* over the horizontal position x and in time t. To exploit this low-aspect ratio, slowly varying nature of the flow we employ the horizontal and vertical length scales L and H and introduce the small parameter δ. The dilute nature of the suspension in the lower layer is characterized by the second small parameter $\epsilon \equiv \varphi_0 \ll 1$ representing the initial spatially uniform volume fraction of particles in the release volume.

We now introduce nondimensional variables according to the following scheme wherein nondimensional variables are indicated by a tilde:

$$\begin{aligned}
x &= L\tilde{x}, \qquad z = H\tilde{z}, \qquad t = \frac{L}{U}\tilde{t}, \qquad h = H\tilde{h},\\
(u_1,u_2) &= U(\tilde{u}_1,\tilde{u}_2), \qquad (w_1,w_2) = H\frac{U}{L}(\tilde{w}_1,\tilde{w}_2),\\
(p_1^*,p_2^*) &= U^2(\rho_1\tilde{p}_1^*,\rho_2\tilde{p}_2^*), \qquad \eta = \frac{U^2}{g}\tilde{\eta},\\
s &\equiv \delta\tilde{s}, \qquad \varphi \equiv \epsilon\tilde{\varphi}, \qquad v_s \equiv \delta\tilde{v}_s,\\
g_1' &\equiv \frac{\rho_2-\rho_1}{\rho_2}g, \qquad g_2' \equiv \frac{\rho_3-\rho_2}{\rho_2}g, \qquad U \equiv (g_1'H)^{1/2}.
\end{aligned} \qquad (2.15)$$

We note that the scaled quantities $\tilde{s}$, $\tilde{\varphi}$, and $\tilde{v}_s$ are now $O(1)$.

Employing this scheme to nondimensionalize the upper layer equations (2.5) and (2.6) gives

$$\frac{\partial u_1}{\partial t} + u_1 \frac{\partial u_1}{\partial x} + w_1 \frac{\partial u_1}{\partial z} = -\frac{\partial p_1^*}{\partial x}, \tag{2.16}$$

$$\delta^2 \left(\frac{\partial w_1}{\partial t} + u_1 \frac{\partial w_1}{\partial x} + w_1 \frac{\partial w_1}{\partial z} \right) = -\frac{\partial p_1^*}{\partial z}, \tag{2.17}$$

where tildes have been dropped from nondimensional quantities for notational convenience.

At this stage we have

$$\frac{\partial p_1^*}{\partial z} = O(\delta^2) \tag{2.18}$$

so that the horizontal pressure gradient in the upper layer will be independent of z and the usual arguments [21] lead to the shallow-water equations for the upper layer, that is, in nondimensional form

$$\frac{\partial u_1}{\partial t} + u_1 \frac{\partial u_1}{\partial x} = -\frac{\partial \eta}{\partial x}, \tag{2.19}$$

$$\frac{\partial}{\partial t}\left(h - \frac{g_1'}{g}\eta \right) + \frac{\partial}{\partial x}\left[\left(h - sf(x) - \frac{g_1'}{g}\eta - 1 \right) u_1 \right] = 0. \tag{2.20}$$

The crucial step leading to shallow-water theory is the sufficient condition that $\partial p_1^* / \partial z \sim 0$ to leading order in a suitable small parameter.

We now nondimensionalize the lower layer equations (2.12) and (2.13) using (2.15) and the convention of suppressing the tilde notation to get

$$\frac{\partial u_2}{\partial t} + u_2 \frac{\partial u_2}{\partial x} + w_2 \frac{\partial u_2}{\partial z} = -\frac{\partial p_2^*}{\partial x}, \tag{2.21}$$

$$\delta^2 \left(\frac{\partial w_2}{\partial t} + u_2 \frac{\partial w_2}{\partial x} + w_2 \frac{\partial w_2}{\partial z} \right) = -\frac{\partial p_2^*}{\partial z} - \epsilon\varphi \frac{g_2'}{g_1'}. \tag{2.22}$$

At this stage, without making some assertions as to the relative sizes of δ and ϵ, we cannot say that u_2 is independent of z and that we are dealing with shallow-water theory. Thus, integration of the continuity equation (2.3), application of the two kinematic boundary conditions, and nondimensional-

ization according to the scheme of (2.15) gives for continuity

$$\frac{\partial h}{\partial t} + \frac{\partial}{\partial x}\left(\int_{-sf(x)}^{h-sf(x)} u_2(x,z,t)\, dz \right) = 0, \tag{2.23}$$

where again tildes are dropped. Employing nondimensional variables in the equation for particle conservation yields

$$\frac{\partial}{\partial t}(h\varphi) + \frac{\partial}{\partial x}\left(\varphi \int_{-sf(x)}^{h-sf(x)} u_2(x,z,t)\, dz \right) + \varphi \frac{v_s}{(g_1' H)^{1/2}} = 0. \tag{2.24}$$

Our nondimensional equations now consist of (2.19)–(2.24) with closure being achieved by means of pressure continuity across the interface at $z = h - sf(x)$, that is,

$$p_2^* = \left(1 - \frac{g_1'}{g}\right)\eta + h - sf(x) \qquad \text{on } z = h - sf(x). \tag{2.25}$$

Our nondimensional equations (2.19)–(2.25) involve five nondimensional parameters with $g_1'/g \equiv \gamma$ measuring the importance of the free surface on the flow dynamics [13], s measuring the importance of bottom topography on flow dynamics, the aspect ratio δ indicating the importance of vertical structure in the flow, and ϵ indicating to what degree the suspended particles will contribute to the vertical structure. This last statement is justified by noting that even for low-aspect ratio flows, when terms $O(\epsilon)$ cannot be neglected we have $p_2^* \sim \epsilon\varphi z$. The fifth nondimensional parameter is the scaled (see (2.15)) settling number $\beta \equiv v_s/(g_1' H)^{1/2} = O(1)$.

We now proceed by assuming the reasonable relation $\epsilon \leq O(\delta^2)$ with $0 < \delta \ll 1$ so that $s = O(1)$. This is a reasonable assumption when one considers that in the experiments of Bonnecaze et al. [12, 18] the initial volume fractions were in the range 1–2%. Then, neglecting terms $O(\epsilon)$ from the lower layer vertical momentum equation (2.22) gives that $\partial p_2^*/\partial z$ is zero to $O(\epsilon)$ and we have the sufficient condition for shallow-water theory. We thus construct our solution in the form

$$\begin{aligned}
u_1 &= u_1^{(0)}(x,t) + O(\epsilon),\\
\eta &= \eta^{(0)}(x,t) + O(\epsilon),\\
h &= h^{(0)}(x,t) + O(\epsilon),\\
u_2 &= u_2^{(0)}(x,t) + O(\epsilon),\\
w_2 &= w_2^{(0)}(x,z,t) + O(\epsilon),\\
p_2^* &= p_2^{*(0)}(x,t) + O(\epsilon),\\
\varphi &= \varphi^{(0)}(x,t) + O(\epsilon),
\end{aligned} \tag{2.26}$$

to get the leading-order shallow-water equations (dropping superscripts from dependent variables)

$$\frac{\partial u_1}{\partial t} + u_1 \frac{\partial u_1}{\partial x} = -\frac{\partial \eta}{\partial x}, \tag{2.27}$$

$$\frac{\partial}{\partial t}(h - \gamma\eta) + \frac{\partial}{\partial x}\left[(h - sf(x) - \gamma\eta - 1)u_1\right] = 0, \tag{2.28}$$

$$\frac{\partial u_2}{\partial t} + u_2 \frac{\partial u_2}{\partial x} = -\frac{\partial p_2^*}{\partial x}, \tag{2.29}$$

$$\frac{\partial h}{\partial t} + \frac{\partial}{\partial x}(hu_2) = 0, \tag{2.30}$$

$$\frac{\partial \varphi}{\partial t} + u_2 \frac{\partial \varphi}{\partial x} = -\beta \frac{\varphi}{h}, \tag{2.31}$$

together with

$$p_2^* = (1-\gamma)\eta + h - sf(x), \tag{2.32}$$

and

$$w_2 = -(z + sf(x))\frac{\partial u_2}{\partial x} - su_2 f'(x). \tag{2.33}$$

For the cases treated by Bonnecaze et al. [12, 18] in which the densities of interstitial and ambient fluids are equal, our $g_1' = 0$ and the scaling adopted above cannot be employed. The appropriate scaling in this case would be that adopted in (2.15) except that now the correct velocity scale used to nondimensionalize time, the various velocity fields, and free surface displacement must be $U \equiv (g'H)^{1/2}$, where now the reduced gravity $g' \equiv (\rho_3 - \rho_1)\epsilon g / \rho_1$ is governed by the initial particle concentration. This scaling of the buoyancy of the current by the initial density difference between the particle-bearing current and the ambient homogeneous fluid is the only one available and is precisely the scaling employed by Bonnecaze et al. [12, 18]. Employing this scheme we find for the nondimensional vertical momentum equation of the lower layer

$$\delta^2\left(\frac{\partial w_2}{\partial t} + u_2\frac{\partial w_2}{\partial x} + w_2\frac{\partial w_2}{\partial z}\right) = -\frac{\partial p_2^*}{\partial z} - \varphi, \tag{2.34}$$

where again tildes are dropped from the nondimensional variables. Thus (2.34) gives

$$\frac{\partial p_2^*}{\partial z} = -\varphi(x,t) + O(\delta^2) \tag{2.35}$$

and we see that when particles drive the flow, as in this case with $\rho_1 = \rho_2$, the hydrostatic condition is violated. This failure to develop a consistent shallow-water theory for this case may be understood in the following way.

First, a consistent shallow-water model can be developed as explained in this article because the buoyancy of the current is scaled relative to the buoyancy contrast between the two fluids and this provides a constant reference value. As the lower layer sediments particles the buoyancy contrast tends to this constant reference value, thereby enabling the precepts of shallow-water theory to apply throughout the region in which sedimentation occurs. On the other hand, a consistent shallow-water theory cannot be achieved in the circumstance under which the particles provide the sole buoyancy contrast. For in this case the buoyancy is scaled with the initial density difference between the particle-bearing current and the surrounding homogeneous fluid. This scaling for the velocity field when combined with the low-aspect ratio nature of the flow demands that the majority of the particles settle out over a nondimensional distance $O(1)$. This means that the buoyancy contrast between the turbidity current and the upper layer will be lost over the same downslope distance resulting in a slowing and deepening of the current, thereby producing significant nonhydrostatic vertical pressure gradients as seen mathematically in (2.35).

In the next section we explore numerically the consequences of our model for the flow and deposition patterns for bottom gravity currents moving over sloping bottoms. Our results are compared with published results where possible.

3. Numerical investigation

3.1. The relaxation scheme

Numerical solutions to the governing equations were obtained using a relaxation scheme proposed recently by Jin and Xin [22] for solving systems of conservation laws. Jin and Xin [22] demonstrated that the scheme is second-order accurate and TVD so that the solutions do not exhibit spurious numerical oscillations and they converge to physical weak solutions. The scheme does not require the evaluation of the eigenvalues of the Jacobian of the flux vector. This is an enormous advantage when dealing with large and complicated systems such as the one that is currently under investigation.

Furthermore, the fact that the solutions are nonoscillatory is an improvement over second-order, finite-difference schemes such as MacCormack's and Lax-Wendroff. This is clearly illustrated in Figure 2 wherein we compare results obtained for a sudden fixed volume release on a sloping bottom using both MacCormack's and the relaxation schemes. In Figure 2, as in all of our numerical work, we choose the function $f(x)$ that describes the bottom topography to be the simple function

$$f(x) = 1 - \exp(-x), \qquad x \geq 0. \tag{3.1}$$

This function, when coupled with the slope parameter s to provide the bottom contour $z = -sf(x)$, gives a reasonable representation of the gentle slopes of the continental rise and abyssal plain. Our boundary conditions will consist of a rigid wall at $x = 0$ and undisturbed fluid in the semi-infinite region to the right of $x = 0$. The results depicted in Figure 2 demonstrate quite clearly the efficacy of the relaxation method. We now outline that method.

For a general one-dimensional system of conservation laws,

$$\frac{\partial \mathbf{u}}{\partial t} + \frac{\partial \mathbf{f}(\mathbf{u})}{\partial x} = \mathbf{0}, \qquad (x,t) \in \mathbb{R} \times \mathbb{R}^+, \mathbf{u} \in \mathbb{R}^n, \tag{3.2}$$

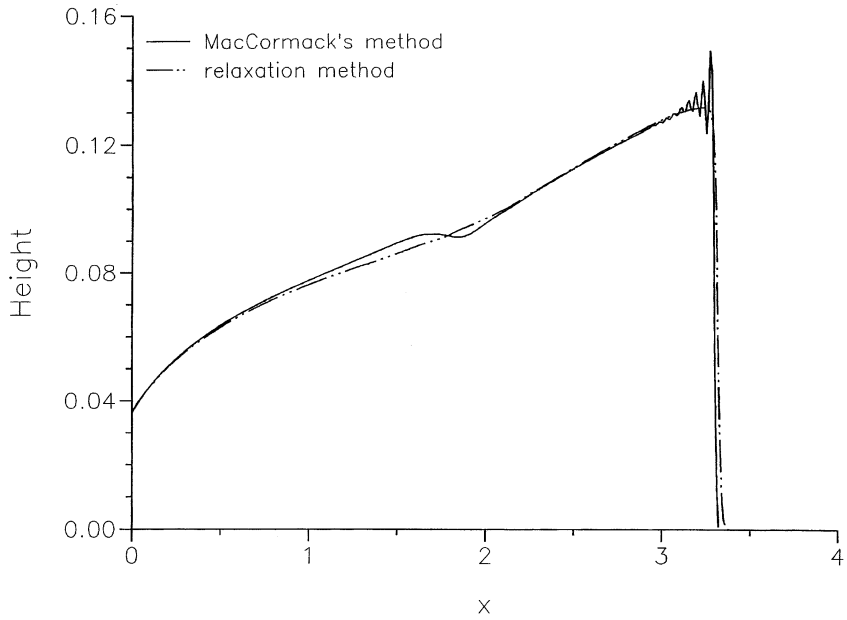

Figure 2. Comparison of numerical results obtained using the relaxation method and MacCormack's method after 5 time units have elapsed from a sudden release with $h_0 = 0.3$, $s = 0.1$, $\gamma = 0.2$, $a = 0.5$, $\Delta x = 0.02$, and $\Delta t = 0.002$.

the *relaxation system* to be solved is defined as

$$\begin{aligned} \frac{\partial \mathbf{u}}{\partial t} + \frac{\partial \mathbf{v}}{\partial x} &= \mathbf{0}, \qquad \mathbf{v} \in \mathbb{R}^n, \\ \frac{\partial \mathbf{v}}{\partial t} + \mathbf{A}\frac{\partial \mathbf{u}}{\partial x} &= -\frac{1}{\epsilon}(\mathbf{v} - \mathbf{f}(\mathbf{u})), \end{aligned} \tag{3.3}$$

where $0 < \epsilon$ is a small constant and $\mathbf{A} = a\mathbf{I}$ is a diagonal matrix such that $0 < a \in \mathbb{R}$. The system is dissipative provided that the condition

$$\lambda^2 < a, \qquad \lambda = \max_{1 \le i \le n} |\lambda_i(\mathbf{u})| \tag{3.4}$$

holds, where $\lambda_i(\mathbf{u})$ is an eigenvalue of the Jacobian matrix $\mathbf{f}'(\mathbf{u})$.

An appropriate numerical discretization of the relaxation system yields an accurate approximation to the original system (3.2) when the relaxation rate ϵ is sufficiently small. A good discretization scheme possesses the correct zero relaxation limit in the sense that as $\epsilon \to 0$ it is a consistent and stable discretization of the original system of conservation laws.

The discretization scheme that is applied to the relaxation system consists of a second-order TVD Runge–Kutta splitting time discretization together with van Leer's [23] MUSCL scheme with the minmod slope limiter for the space discretization. The MUSCL scheme provides second-order accuracy and eliminates oscillations around discontinuities by combining a piecewise linear interpolation with Godunov's method. The implicit Runge–Kutta time discretization overcomes the stability difficulties generated by the stiffness of the relaxation system.

It is shown in [22] that this scheme has the correct zero relaxation limit. Hence choosing $\epsilon = O((\Delta t)^3)$, where Δt is the time increment, and ignoring the $O(\epsilon/\Delta t)$ terms, the scheme becomes independent of the artificial parameters $\mathbf{v}$ and ϵ and is thus a second-order scheme for the original system (3.2).

It should be mentioned, however, that the scheme is still dependent upon the parameter a, the upper bound on the eigenvalues. It turns out that too large values of a lead to some undesirable smearing of discontinuities. Since the complexity of our system does not readily allow us to obtain analytic expressions for the eigenvalues, we experimented with various values of a and found that the scheme yields stable results with sharp resolution if $a = 0.5$. This is clearly demonstrated in Figure 3 where the height profile of the underflow arising from a sudden release on a sloping bottom is depicted. For these numerical runs we have chosen the initial fractional depth $h_0 = 0.9$ in order to have both the rear and forward shocks to resolve. At this

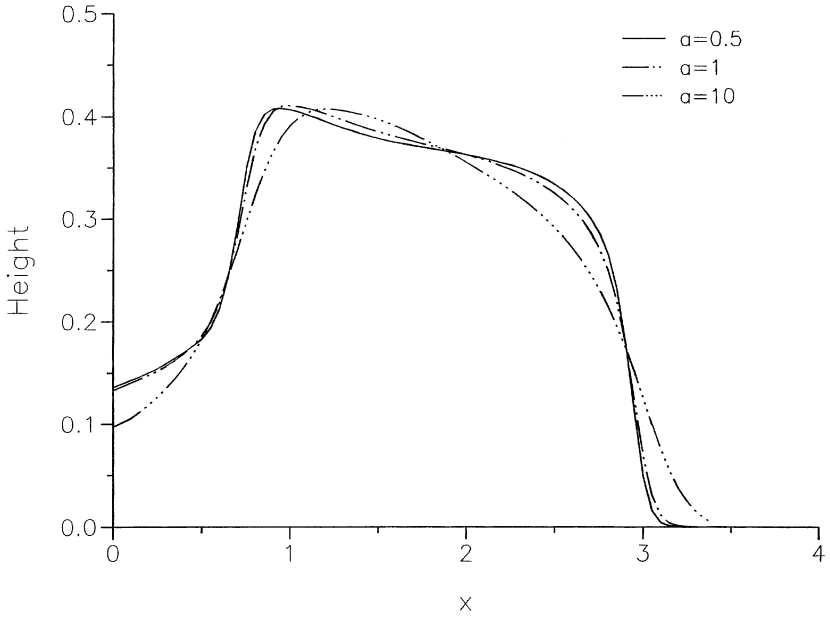

Figure 3. Effect of the eigenvalue bound on shock resolution for $h_0 = 0.9$, $s = 0.1$, $\gamma = 0.2$, $\Delta x = 0.05$, and $\Delta t = 0.002$ at $t = 3$.

point in the evolution of the bottom gravity current, the height profile looks very much as it would for the horizontal bottom studied in [13]. The smearing of discontinuities as a is increased is shown clearly in Figure 3.

3.2. Numerical results

The effect of the variable slope on the bottom gravity current is clearly exhibited by contrasting the time evolution of the two cases depicted in Figures 4 and 5. Both of these cases correspond to a sudden release with initial fractional depth $h_0 = 0.3$, with Figure 4 giving the time evolution for a gravity current on a horizontal bottom and Figure 5 showing the gravity current moving over the variable slope bottom. This value for the initial fractional depth was chosen here to highlight an essential difference between these two flows. We know from previous studies [13] that for this value of the initial fractional depth and a horizontal bottom, the reverse flow in the upper and lighter fluid is inadequate for the generation of the rear internal bore or hydraulic jump that can be seen for $h_0 \gtrsim 0.7$. Instead, for this value of h_0 the disturbance from the end wall at $x = 0$ takes the form of a long wave of depression as the current slumps irrevocably toward its self-similar form as shown in [13]. This is clearly demonstrated in Figure 4 where we should also observe that the bottom gravity current remains in contact with the end wall for all time.

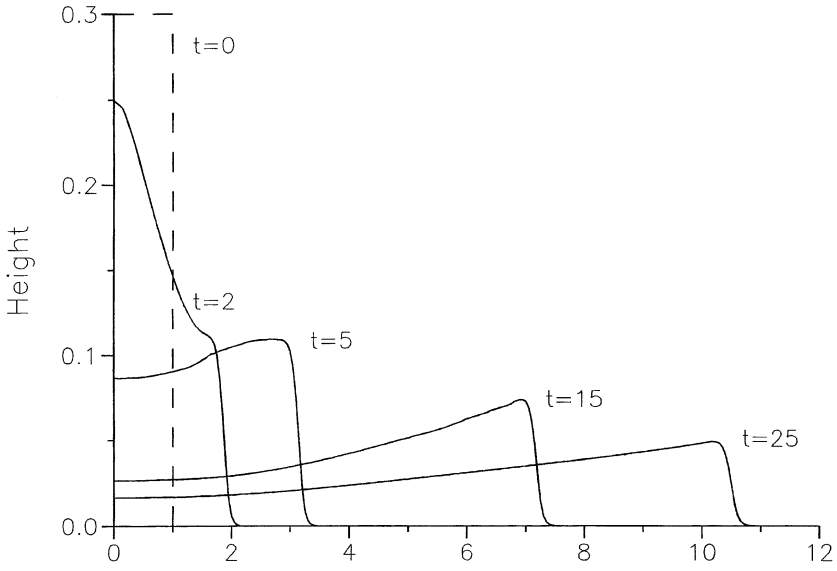

Figure 4. Time evolution of gravity current with $h_0 = 0.3$, $s = 0$, $\gamma = 0.2$, $\Delta x = 0.05$, and $\Delta t = 0.002$.

The time evolution of the gravity current arising from a sudden release on a sloping bottom, as depicted in Figure 5, has several interesting features to distinguish it from the current on a flat bottom. First, but not necessarily most importantly, the dense bottom current loses contact with the endwall at $t \approx 8$. This is clearly the effect of the slope on the current. In the absence of slope the collapse of the dense fluid forces it to remain in contact with the end wall as it spreads out to eventually cover the entire bottom. However, when there is a sloping bottom the motion induced down the slope by the component of gravity may be greater than the rate of spread due to collapse with the net result that the current will disengage from the end wall. This can be observed in the evolution of the bottom gravity current depicted in Figure 5.

A second feature that clearly differentiates currents on sloping bottoms from those on horizontal ones is that a second shock can form even when the fractional release depth $h_0 < 0.5$. This shock is seen to have formed by $t \approx 25$ in Figure 5. This shock formation is a result of the sloping bottom and our relaxation method is very adept at tracking it. One can envision this shock as forming because the parcel of fluid at the trailing edge of the bottom surge is on a steeper slope than the fluid to its right and so will be accelerated relative to that fluid. This has the effect of creating a compressive zone at the trailing edge that will lead to wave breaking.

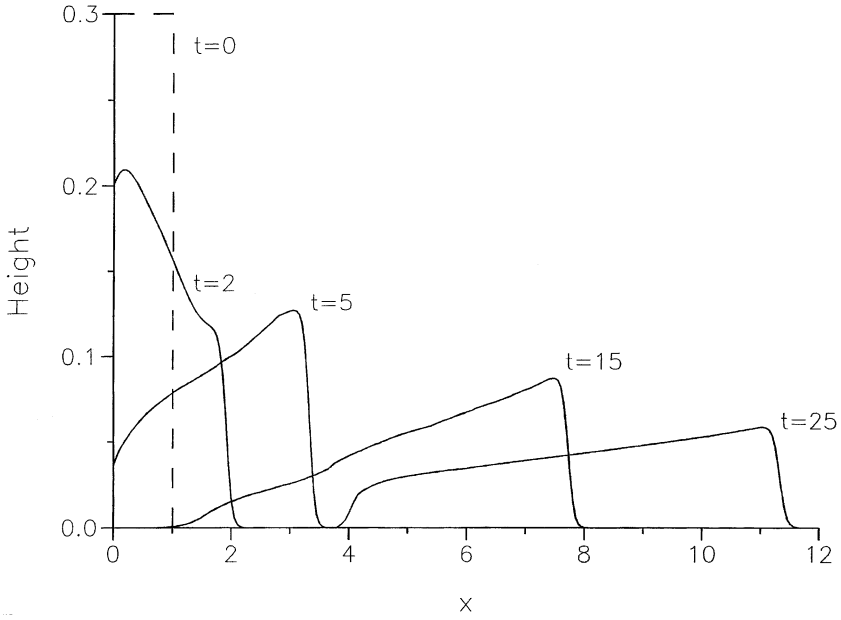

Figure 5. Time evolution of gravity current with $h_0 = 0.3$, $s = 0.1$, $\gamma = 0.2$, $\Delta x = 0.05$, and $\Delta t = 0.002$.

In Figure 6 we explore the end wall separation phenomenon for sudden releases on sloping bottoms in considerable detail. In this figure are plotted separation times versus slope parameter s for two very different release heights. The trend toward an infinite separation time as the slope parameter $s \to 0$ is clearly demonstrated for both release heights. The tendency of the separation time to have higher values over the entire range of the slope parameter when the release height of the fixed volume is greater can be seen here also, although this dependence on release height is relatively weak.

Figures 7 and 8 show the time evolution for the bottom gravity currents produced by a sudden release volume of fractional depth $h_0 = 0.9$ on horizontal and sloping bottoms, respectively. The evolution to self-similarity for the horizontal bottom as depicted in Figure 7 can be compared with that shown in Figure 4. This shows clearly the effect of initial fractional depth on the evolution to self-similarity. When the initial fractional depth is close to unity as in Figure 7, the vigorous reverse flow in the upper fluid produces, on interacting with the end wall, an internal hydraulic drop, which is not generated when $h_0 = 0.3$ as in Figure 4.

In both Figures 7 and 8 we can see the internal bore produced when the reverse flow interacts with the end wall at $x = 0$. This internal bore travels to the right faster than the front and, in both cases, overtakes the front.

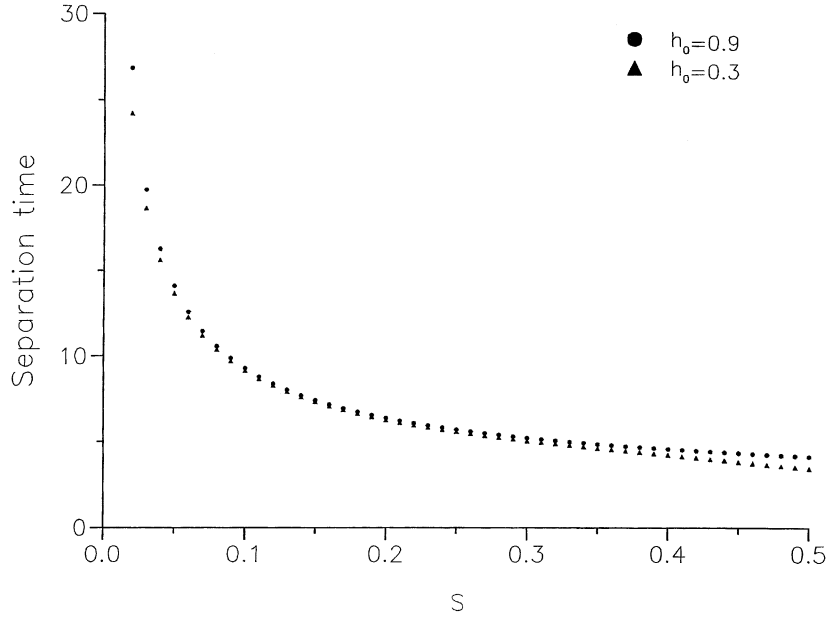

Figure 6. Nondimensional separation time as a function of s for $h_0 = 0.3$ and $h_0 = 0.9$.

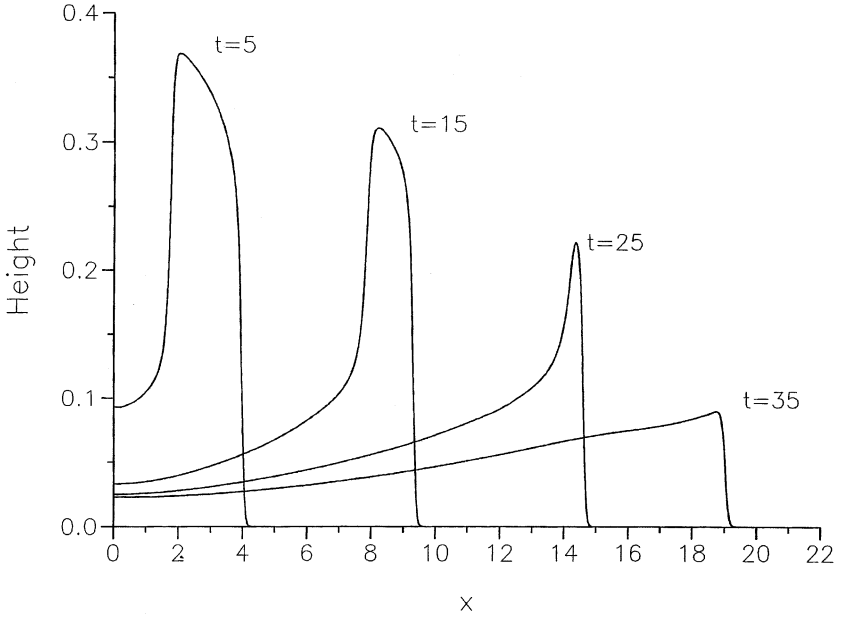

Figure 7. Time evolution of gravity current with $h_0 = 0.9$, $s = 0$, $\gamma = 0.2$, $\Delta x = 0.05$, and $\Delta t = 0.002$.

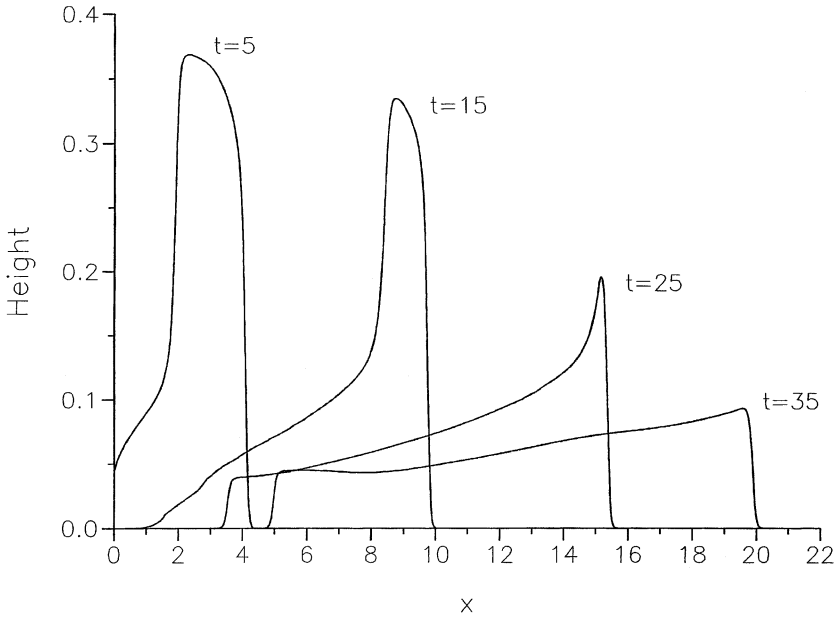

Figure 8. Time evolution of gravity current with $h_0 = 0.9$, $s = 0.1$, $\gamma = 0.2$, $\Delta x = 0.05$, and $\Delta t = 0.002$.

However, in Figure 8 we see a third shock that is not present in Figure 7. This shock is produced owing to the creation of a compressive zone at the rear of the gravity surge on the sloping bottom.

In Figure 9 we demonstrate the effect that initial fractional depth has on gravity current structure at a time prior to the slope-generated rear shock. What is shown in Figure 9 is somewhat like that which would be observed for a current on a horizontal flat bottom in that the shock that is formed in the interior due to vigorous backflow in the upper fluid depends on the value of the initial fractional depth. This depth must be greater than some minimum value that is definitely greater than 0.5. The flow on the sloping bottom is, however, seen to differ from that on the horizontal one in that the gravity surge separates from the end wall. This separation occurs prior to the slope-induced rear shock being formed.

In the sequence of figures numbered 10 through 13 we explore the critical role played by the slope parameter in end-wall separation of the bottom gravity current. All of these figures are for a fractional release depth $h_0 = 0.9$ with the bottom current being depicted at $t = 40$, 50, 60, 70, and 80 nondimensional time units from flow initiation. Figures 10 and 11 are for values of the slope parameter $s = 0.015$ and $s = 0.02$, respectively. These figures show clearly that for these small values of s there exists an approximate balance between the tendency of the current to flow down the slope

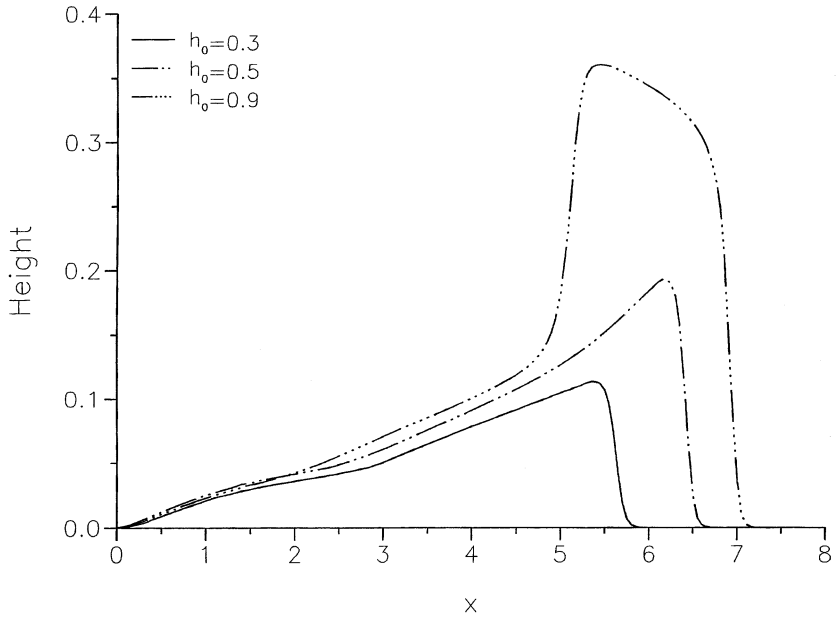

Figure 9. Dependence of gravity current structure on initial fractional depth h_0. Here $t = 10$, $s = 0.1$, and $\gamma = 0.2$.

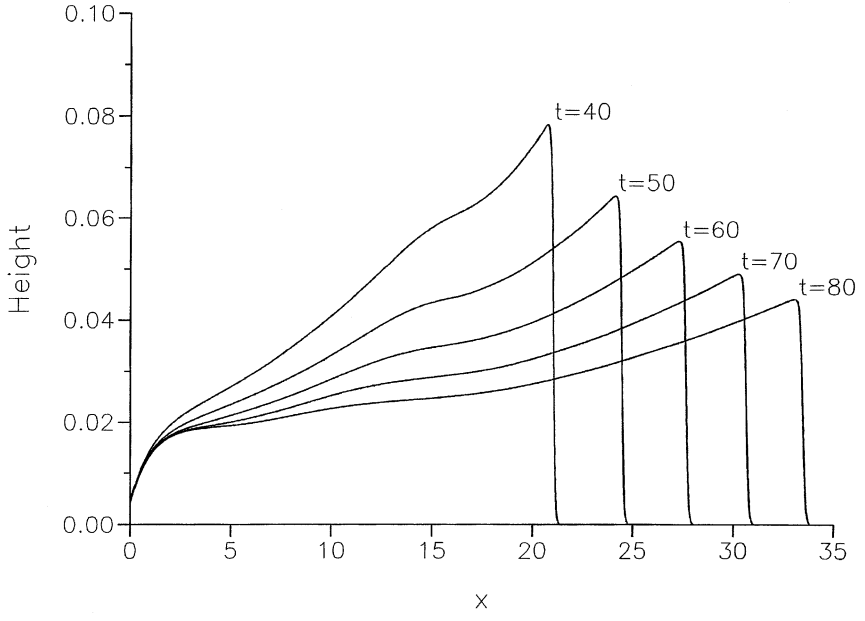

Figure 10. Time evolution of gravity current for large times with $h_0 = 0.9$, $s = 0.015$, $\gamma = 0.2$, $\Delta x = 0.05$, and $\Delta t = 0.002$.

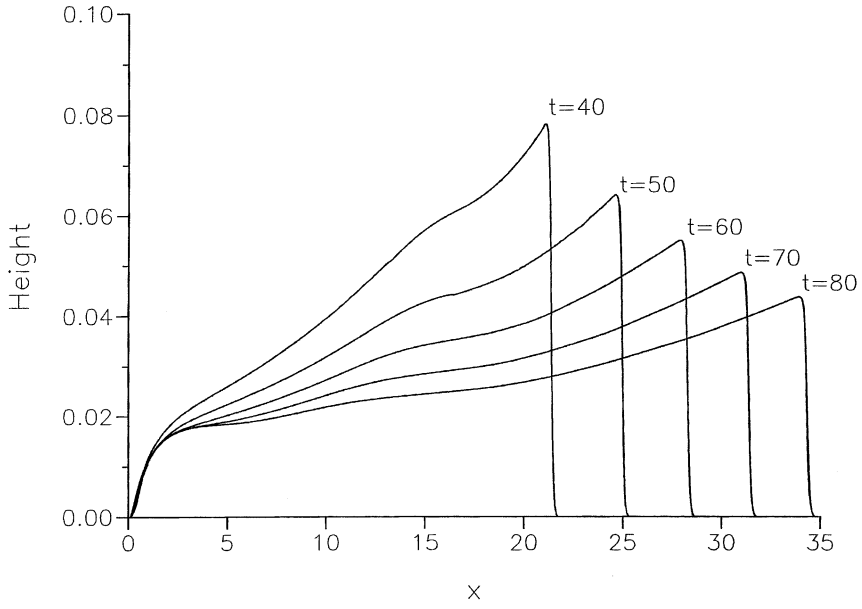

Figure 11. Time evolution of gravity current for large times with $h_0 = 0.9$, $s = 0.02$, $\gamma = 0.2$, $\Delta x = 0.05$, and $\Delta t = 0.002$.

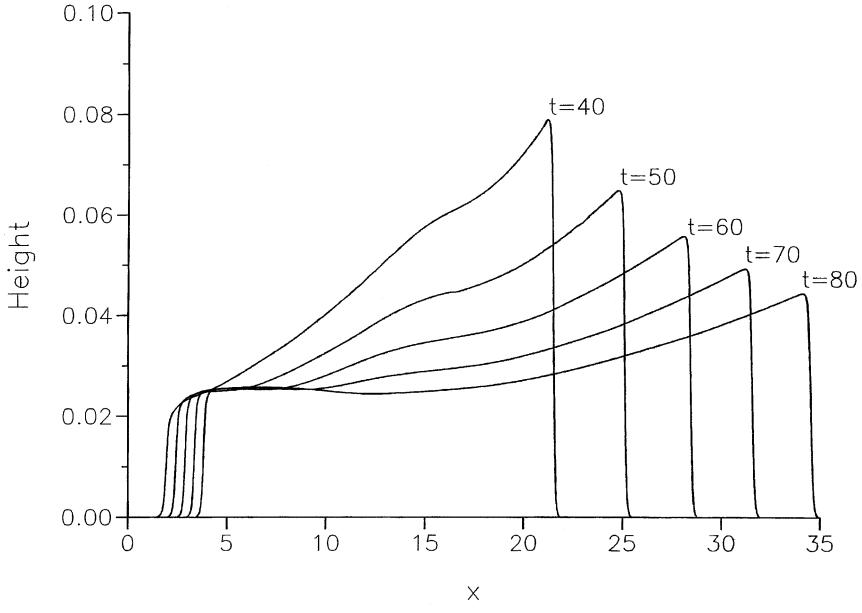

Figure 12. Time evolution of gravity current for large times with $h_0 = 0.9$, $s = 0.04$, $\gamma = 0.2$, $\Delta x = 0.05$, and $\Delta t = 0.002$.

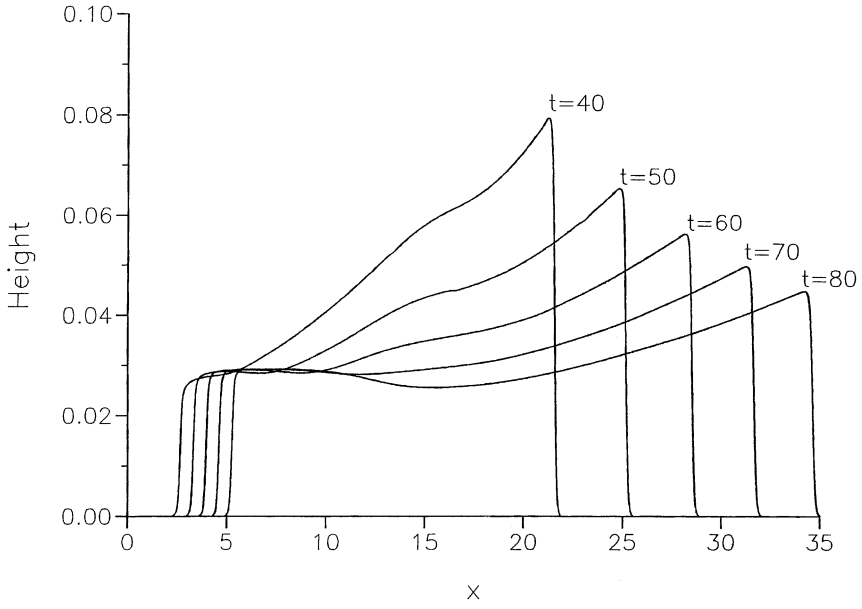

Figure 13. Time evolution of gravity current for large times with $h_0 = 0.9$, $s = 0.05$, $\gamma = 0.2$, $\Delta x = 0.05$, and $\Delta t = 0.002$.

and its wallward movement due to self-collapse. It is this balance that creates the approximately steady state at the end wall that is observed in these figures. With increasing values of the slope parameter as depicted in Figures 12 and 13 the regime is reached in which the downslope flow overcomes the self-collapse and the current separates from the end wall and moves downslope as a gravity surge [5].

In Figure 14, where the slope parameter has the value $s = 0.02$, we have depicted a number of numerical experiments designed to study the time of separation of the current from the end wall. Again, in this case we see that the current separates from the end wall to form a compactly supported gravity surge whose rate of thinning will be less than that associated with the current on a horizontal bottom.

We now present numerical results for the downslope particle deposition patterns. In Figures 15–19 the nondimensional (scaled) density of deposit is plotted both as a function of the downslope distance for large times (Figures 15–17) and as a function of time at both fixed downslope position (Figure 18) and several different downslope positions (Figure 19).

Here, for the purpose of defining the density of the deposit we revert to the tilde notation for nondimensional quantities. We denote the nondimensional density of deposit by $\tilde{m}$ and it is related to the dimensional density m (mass/area) by $m = M\tilde{m}$, where $M = \rho_3 L \epsilon$ with ϵ the previously defined

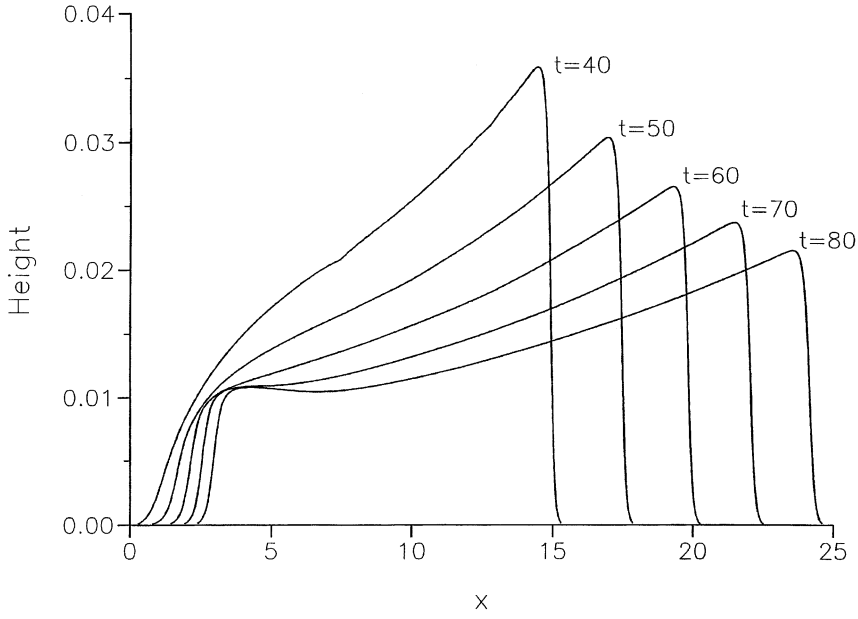

Figure 14. Time evolution of gravity current for large times with $h_0 = 0.3$, $s = 0.02$, $\gamma = 0.2$, $\Delta x = 0.05$, and $\Delta t = 0.002$.

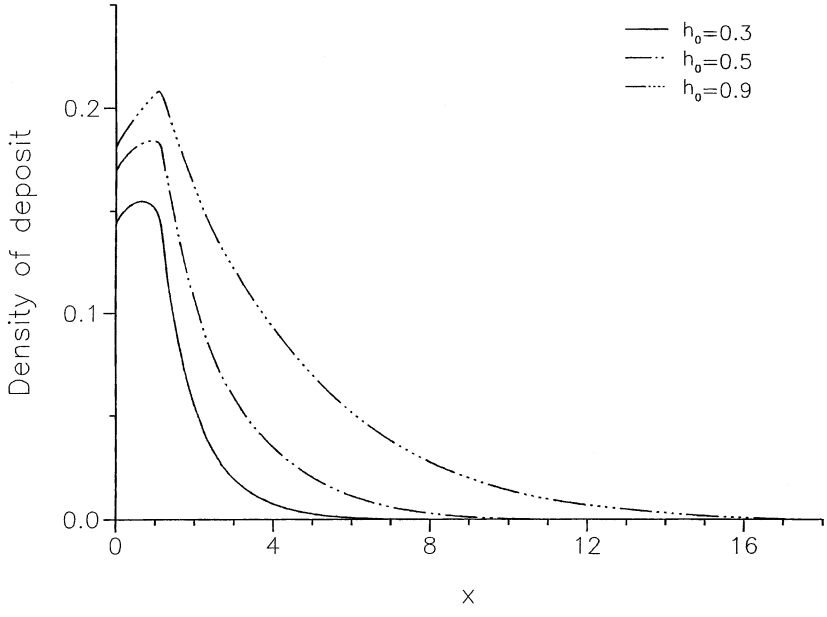

Figure 15. Nondimensional density of deposit for various values of h_0 with $s = 0.1$ and $\beta = 0.05$.

constant initial volume fraction of particles. Then

$$m = \int_0^t \rho_3 \tilde{v}_3 \varphi \, dt$$

$$= T \int_0^{\tilde{t}} \rho_3 \tilde{v}_s \epsilon \tilde{\varphi} \, dt$$

$$= M \int_0^{\tilde{t}} \frac{\tilde{v}_s \tilde{\varphi}}{\sqrt{g_1' H}} \, dt$$

so that

$$\tilde{m} \equiv \int_0^{\tilde{t}} \frac{\tilde{v}_s \tilde{\varphi}}{\sqrt{g_1' H}} \, dt, \tag{3.5}$$

where $\tilde{v}_s$ is the dimensional scaled settling velocity as defined previously.

Figures 15 and 16 display the effects of initial fractional depth of the release volume and bottom slope on the depositional pattern. In each of these figures the vertical axis is the complete time integral for $\tilde{m}$ in (3.5). In Figure 15 we can clearly see the effect of varying the initial volume of the particle suspension by varying its initial fractional depth. The greater the depth and hence volume of suspension the greater will be the eventual density of the bottom deposit. Also the downslope extent of the deposit increases with increasing values of the fractional depth. This is certainly in accord with what our model equation (2.31) says about deposition rate being inversely proportional to current depth. It is interesting to note that the global maxima for each of the density curves in Figure 15 is shifted downslope from the end wall. This is caused by the presence of bottom slope and the fact that the sediment-bearing gravity current disengages from the end wall.

Figure 16 demonstrates that the effect of increasing the slope parameter s will be to shift particle deposits somewhat downstream thereby causing a reduction in particle deposition near $x = 0$. We also see the shift in the maxima of the density of deposit with increasing slope and, in particular, we see the maximum occurring at the end wall in the absence of slope.

In Figure 17 we have plotted the density of deposit as a function of the downslope distance for three different settling numbers β. Several things are apparent from this figure. First, the effect of the slope is to shift the maximum density of deposit for each β in the downslope direction. This shift is a result of end-wall separation of the gravity current. With decreasing values of β the observed tendency is for the density of the deposit to be

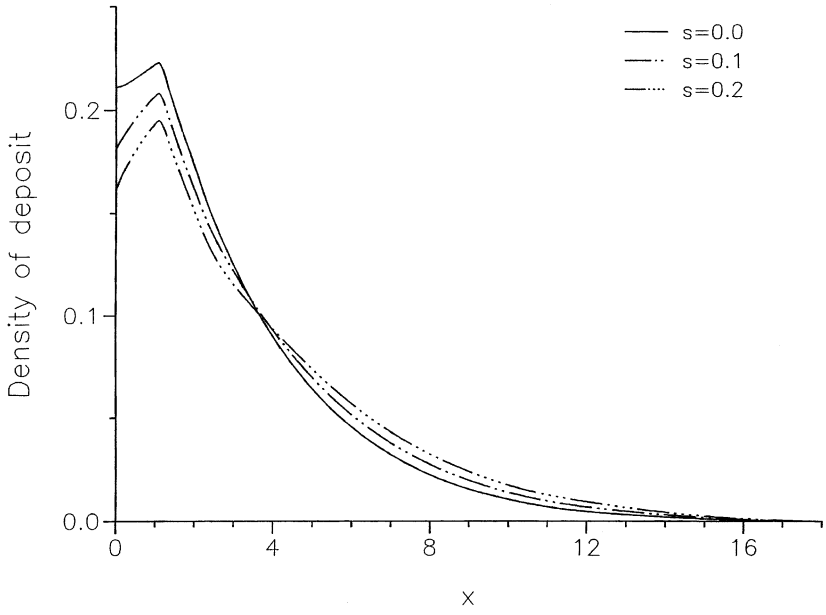

Figure 16. Nondimensional density of deposit for various values of s with $h_0 = 0.9$ and $\beta = 0.05$.

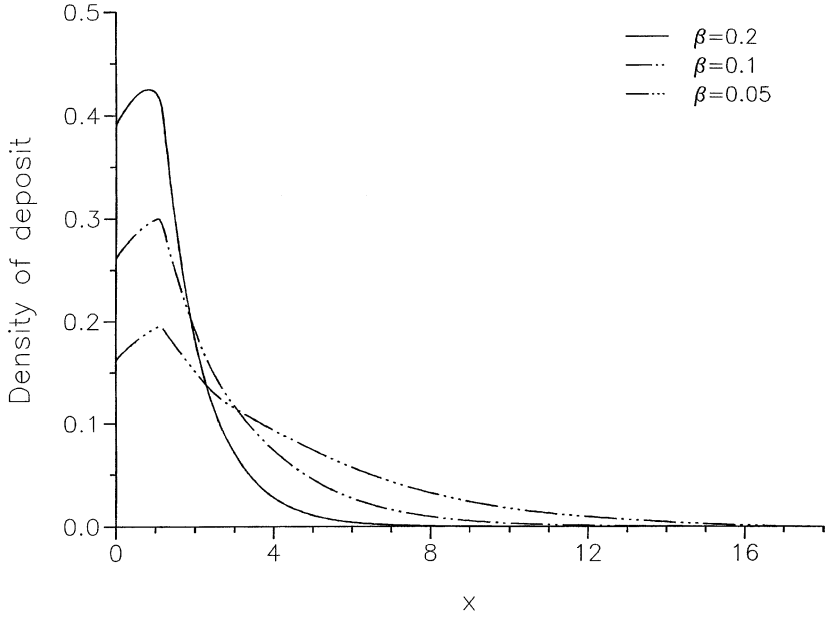

Figure 17. Nondimensional density of deposit as a function of x for various values of β with $s = 0.2$, $h_0 = 0.9$, and $\gamma = 0.2$.

shifted downslope as the suspended particles are sedimented at a slower rate and hence advected further by the flow. This trend is in agreement with experimental observations [1].

In Figure 18 we examine the effect of varying the scaled nondimensional settling velocity β on the density of the deposit at the fixed station $x = 0.5$ as a function of time. We find that at small values of the post-release time the density of deposited particles with the larger settling velocity increases at the greater rate. We also see that at this station the maximum density of deposit for the three different settling velocities is reached at $t \approx 4$ and that this maximum is an increasing function of β. The fact that our model predicts this rate of deposit behavior is in accord with the field observations that show graded beds with larger particles being dominant in the lower layers [1].

In Figure 19 we have depicted the density of deposit at various downslope stations as a function of time. We see clearly the passage of the particle-bearing gravity current in its depositional phase. For the station located at $x = 0.5$, which is at the midpoint of the base of the release volume, particles are deposited from the time of release of the fixed volume with the density of deposit rising rapidly to achieve its maximum value at $t \approx 15$, by which time the separated gravity current has gone beyond this station. For the station at downslope position $x = 4.0$ particles start being deposited when

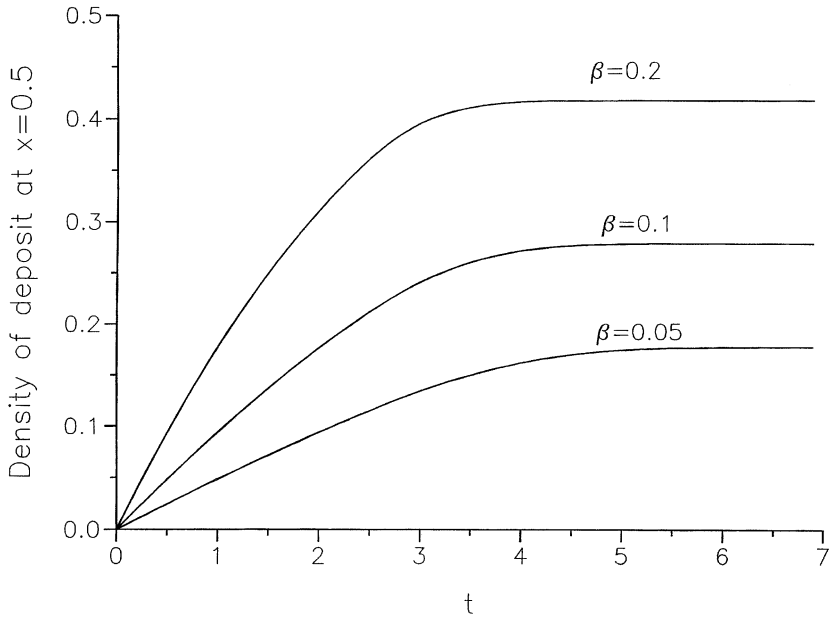

Figure 18. Nondimensional density of deposit at $x = 0.5$ as a function of time for various values of β, with $s = 0.2$, $h_0 = 0.9$, and $\gamma = 0.2$.

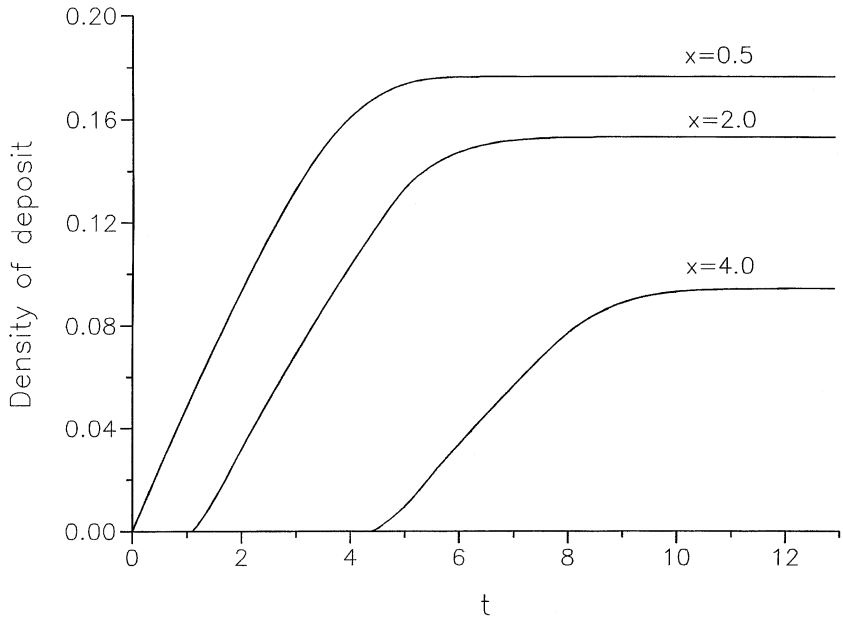

Figure 19. Nondimensional density of deposit as a function of time at various values of x with $\beta = 0.05$, $s = 0.2$, $h_0 = 0.9$, and $\gamma = 0.2$.

the front of the advancing gravity current reaches that station. Their rate of deposition here is slower than at either $x = 0.5$ or $x = 1.2$, reflecting the fact that a proportion of particles have already settled, thereby reducing the volume fraction of particles, as well as the fact that for early times at this station the current is thicker, thereby lowering the rate of deposit.

4. Discussion

In this article we have developed a theory for monodisperse, noneroding, particle-suspension gravity currents on a variably sloping bottom under a free surface in the depositional regime. Our model equations provide a shallow-water theory for this two-layer fluid system having the variable density lower layer. Sufficiency conditions for the validity of our model are that both the aspect ratio δ and the initial volume fraction of particles ϵ be small with $\epsilon \leq O(\delta^2)$. Our development shows rigorously that when the two-layer shallow-water theory is applicable, the fluid momentum equations will be decoupled from the equation describing the conservation of suspended particles. This result was anticipated by Dade and Huppert [19] in an ad hoc analysis of nonentraining suspension-driven gravity surges on horizontal surfaces.

The analysis presented in this article demonstrates that turbidity or particle-driven flows cannot be described in terms of a consistent shallow-water theory. It would therefore appear that the conclusions concerning reversing buoyancy effects in sediment-laden gravity currents as described in [17] and based upon a "shallow-water" theory are dynamically incorrect. This conclusion must then also apply to the theoretical results that are presented in [12, 18] and based upon the same inconsistent development of shallow-water theory.

Using our model we were able to show the differences between flow from a sudden release on a sloping bottom and that on a flat horizontal one. These differences are depicted clearly in our numerical studies as presented in the collection of figures. We see that the flow on a sloping bottom will separate from the end wall and move down the slope in the form of a compact gravity surge. On a horizontal flat surface the gravity current will remain in constant contact with the end wall. Another major difference between flows on horizontal and sloping bottoms is the spontaneous generation of a rear shock in flows on sloping bottoms. This shock forms for all values of the initial fractional depth of the release volume. This is in contrast to the internal hydraulic drop formed in flows on both horizontal and sloping bottoms due to the interaction of the reverse flow with the end wall. The generation of this internal bore requires an initial fractional depth for the release volume greater than 0.7.

Acknowledgments

The authors T.B.M. and G.E.S. are grateful for financial support in the form of individual Research Grants from the Natural Sciences and Engineering Research Council of Canada. We also thank Patrick Montgomery for many stimulating conversations.

References

1. G. V. Middleton, Sediment deposition from turbidity currents, *Annu. Rev. Earth Planet. Sci*. 21:89–114 (1993).
2. S. J. D. D'Alessio, T. B. Moodie, J. P. Pascal, and G. E. Swaters, Intrusive gravity currents, *Stud. Appl. Math*. 98:19–46 (1997).
3. P. J. Montgomery and T. B. Moodie, Analytical and numerical results for flow and shock formation in two-layer gravity currents, *J. Austr. Math. Soc. (Series B)* 39:1–23 (1998).
4. J. E. Simpson, *Gravity Currents*: *In the Environment and the Laboratory*, Ellis Horwood, 1987.
5. W. B. Dade, J. R. Lister, and H. E. Huppert, Fine-sediment deposition from gravity surges on uniform slopes, *J. Sediment. Res. A* 64:423–432 (1994).

6. T. von Kármán, The engineer grapples with nonlinear problems, *Bull. Am. Math. Soc.* 46:615–683 (1940).

7. T. B. Benjamin, Gravity currents and related phenomena, *J. Fluid Mech.* 31:209–248 (1968).

8. J. B. Klemp, R. Rotunno, and W. C. Skamarock, On the dynamics of gravity currents in a channel, *J. Fluid Mech.* 269:169–198 (1994).

9. D. P. Hoult, Oil spreading on the sea, *Ann. Rev. Fluid Mech.* 4:341–368 (1972).

10. T. K. Fannelop and G. D. Waldman, Dynamics of oil slicks, *AIAA J.* 10:506–510 (1972).

11. H. E. Huppert, The propagation of two-dimensional and axisymmetric viscous gravity currents over a rigid horizontal surface, *J. Fluid Mech.* 121:43–58 (1982).

12. R. T. Bonnecaze, H. E. Huppert, and J. R. Lister, Particle-driven gravity currents, *J. Fluid Mech.* 250:339–369 (1993).

13. S. J. D. D'Alessio, T. B. Moodie, J. P. Pascal, and G. E. Swaters, Gravity currents produced by sudden release of a fixed volume of heavy fluid, *Stud. Appl. Math.* 96:359–385 (1996).

14. J. W. Rottman and J. E. Simpson, Gravity currents produced by instantaneous releases of a heavy fluid in a rectangular channel, *J. Fluid Mech.* 135:95–110 (1983).

15. R. J. LeVeque, *Numerical Methods for Conservation Laws*, Birkhäuser, 1992.

16. R. E. Grundy and J. W. Rottman, The approach to self-similarity of the solutions of the shallow-water equations representing gravity-current releases, *J. Fluid Mech.* 156:39–53 (1985).

17. R. S. J. Sparks, R. T. Bonnecaze, H. E. Huppert, J. R. Lister, M. A. Hallworth, H. Mader, and J. Phillips, Sediment-laden gravity currents with reversing buoyancy, *Earth Planet. Sci. Lett.* 114:243–257 (1993).

18. R. T. Bonnecaze, M. A. Hallworth, H. E. Huppert, and J. R. Lister, Axisymmetric particle-driven gravity currents, *J. Fluid Mech.* 294:93–121 (1995).

19. W. B. Dade and H. E. Huppert, A box model for non-entraining suspension-driven gravity surges on horizontal surfaces, *Sedimentology* 42:453–471 (1995).

20. G. Parker, Y. Fukushima, and H. M. Pantin, Self-accelerating turbidity currents, *J. Fluid Mech.* 171:145–181 (1986).

21. J. Pedlosky, *Geophysical Fluid Dynamics*, 2nd ed., Springer-Verlag, 1986.

22. S. Jin and Z. Xin, The relaxation schemes for systems of conservation laws in arbitrary space dimensions, *Comm. Pure Appl. Math.* 48:235–276 (1995).

23. B. van Leer, Towards the ultimate conservative difference schemes. V. A second-order sequel to Godunov's method, *J. Comput. Phys.* 32:101–136 (1979).

University of Alberta, Edmonton

(Received April 16, 1997)